Contents list available at IJRED website

Int. Journal of Renewable Energy Development (IJRED)

Journal homepage: http://ejournal.undip.ac.id/index.php/ijred

Research Article

Numerical Performance Analyses of Different Airfoils for Use in Wind Turbines

Hasan Duz* and Serkan Yildiz

Batman University, Technology Faculty, Automotive Engineering, Turkey

ABSTRACT. This study numerically investigated different types of high-performance airfoils in order to increase the efficiency of wind turbines. Performances of five airfoil types were numerically simulated at different attack angles (0 ° <α <20 °) and at different wind speeds (4, 8, 16 and 32 m/s). Numerical analysis shows that all airfoils achieve the highest performance at attack angles between 4° and 7°. Results also show that the performance of all airfoils increases in direct proportion to increase in wind speed with a low gradient. A new hybrid airfoil was generated by combining lower and upper surface coordinates of two high-performance airfoils which achieved the better results in pressure distribution. Numerical analysis shows that the hybrid airfoil profile performs up to 6% better than other profiles at attack angles between 4° and 7° while it follows the maximum performance curves closely at other attack angles.

Keywords: wind speed, wind turbine, attack angle, airfoil performance, airfoil lift and drag

Article History: Received January 16th 2018; Received in revised form June 5th 2018; Accepted June 15th 2018; Available online
How to Cite This Article: Duz, H and Yildiz, S. (2018) Numerical Performance Analyses of Different Airfoils for Use in Wind Turbines. *Int. Journal of Renewable Energy Development*, 7(2), 151-157.
https://doi.org/10.14710/ijred.7.2.151-157

1. Introduction

Due to technological advances, the demand for energy increases rapidly throughout the world. Fossil fuels are the main sources of energy utilized to meet the demand imposed by today technology. However, the use of fossil fuels pollutes the environment. Carbon dioxide, which is a product of the burning of fossil fuels, is a greenhouse gas and absorbs more solar energy than other air ingredients. Caused by the excessive accumulation of greenhouse gases in the atmosphere, the global warming is a serious problem of the century in which we live as shifting seasons and the melting of ice in the polar regions are directly linked to warmer global temperatures. If fossil fuel consumption is not stopped or curtailed on time, the world will face serious environmental disasters in the future. Scientists who are aware of this massive problem are now exploring ways and means of using renewable energy sources.

Today, one of the most common renewable sources of energy is the wind energy, which has been used for a long time to power ships and to operate mills. The wind energy is regarded as an appropriate and important source of energy, especially since it contributes to the socio-economic development of rural areas. Researchers, today, conduct many studies on wind energy to make it more cost effective and efficient. It is quite obvious that the world's energy giants will definitely be those that run the renewable energy sector in the future.

Electricity in wind turbines is generated by rotor motion. Lift force acting on airfoil walls results in rotor motion. The ratio of lift force to drag force corresponds to airfoil performance. So that the wind energy conversion efficiency is directly associated to airfoil performance, indicating that using high performance airfoils on wind turbines is the most cost-effective way of generating wind energy. There are many experimental and numerical studies on flows over airfoils to be used in wind turbines. Some of those studies are briefly summarized below.

Tangler et al. (1995) conducted an experimental study on NREL-series airfoil profiles for horizontal axis wind turbines in order to evaluate lift force and drag force. Selig et al. (2003) experimentally investigated E387, FX 63-137 (C), S822 (B), S834, SD2030 (B) and SH3055 airfoil profiles in a wind tunnel to measure the aeroacoustics and aerodynamics in order to achieve high efficiency in silent and small wind turbines for use in low speed wind areas in America. Geissler (2003) carried out a numerical study on the vibrational effect of the transonic flow over an NLR-7301 airfoil simulated by the Spalart-Allmaras turbulence model. Using the large Eddy Simulation (LES) method, Dahlstrom et al. (2000) analyzed the applicability of LES on flows over airfoils. Bertagnolio et al. (2005) employed the detached eddy simulation (DES) method to simulate flows over RISO-B1-18 airfoils for use on wind turbines. Parezanovic et al. (2006) experimentally tested NACA 63 (2) 215, FFA-W3-211 and A-AIRFOIL profiles to create

* Corresponding author: hasan.duz@batman.edu.tr (Phone:+905419726088)

© IJRED – ISSN: 2252-4940, July 15th 2018, All rights reserved

different airfoil profiles for wind turbines in order to determine the changes in C_L and C_D values with attack angle. Bekka et al. (2009) also simulated flow over NACA0012 at low attack angles to test Spalart-Allmaras, Baldwin-Lomax, k-ω and k-ω SST turbulence models. Ji et al. (2012) reduced the flow to two-dimensional flow in order to numerically analyze wind turbine airfoil performance. They applied different turbulence models to examine lift and drag coefficients, and compared them with experimental results. Güleren et al. (2011) conducted a numerical study on six different airfoil profiles for use in wind turbines at high Reynolds numbers and low attack angles ($0^o \leq \alpha \leq 20^o$). Results indicated that CLARK Y airfoil profile achieved the best performance at different attack angles. They concluded that the validity of the solutions depended on the attack angle for each airfoil profile. Yılmaz et al. (2016) measured the aerodynamic performances of three commonly used airfoil profiles (S826, NACA 4415 and NACA 63-415) in a subsonic wind tunnel test. Experiments were perfor-med at wind speeds of 6 to 8 m/s and attack angles ranging from -4^o to 6^o. They found that the efficiency of NACA 63-415 airfoil profile for wind turbines running at low speeds and a wide range of attack angles was better than those of others. Similar studies also numerically simulated the flow over airfoils and performed flow analysis (Jang et al. (1998), Bermudez et al. (2002)).

The studies above implemented various experimental and numerical methods to simulate the flow over different types of airfoils to investigate their performance in order to design more efficient wind turbines. These studies indicate that the flow over airfoils is a complex type of flow. Since Reynols Averaged Navier Stokes (RANS) equations is not capable of predicting unsteady vortex flow motion, (LES) and direct numerical simulation (DNS) were used to simulate the flow over airfoils to enhance the vortex flow motion in an unsteady turbulent flow field at high attack angles. Three methods were applied to transiently simulate the turbulent flow field. However, the computational cost of these methods is very high due to high mesh resolution and high time steps. On the other hand, the numerical solution of a turbulent flow field is simple as it does not depend on time, and the computational cost is very low. The governing flow equations for the time-mean flows are converted to RANS equations. However, the solution of the Reynolds stresses existed in RANS equations is achieved using semi-empirical turbulent models. It is therefore crucial to choose an appropriate turbulent model for flows over an airfoil.

Numerous experimental and numerical studies have been performed so far in order to design more efficient wind turbines. It is evident that it is not cost effective to use numerical solutions for flows over airfoils in order to find an apropriate profile from available airfoil profiles. To this end, five airfoil profiles were selected online from available airfoil profiles (UIUC Applied Aerodynamics Group (2017)). The selected airfoils were numerically tested to evaluate their performance at different attack angles and different wind speeds. Numerical analysis yielded the types of airfoils with the best performance. In addition, the two airfoil profiles with the best pressure distribution on the walls were used to generate a new hybrid airfoil profile. The new hybrid airfoil was numerically tested for the assessment of its performance. It showed better performance than the other profiles and proved to be stable.

Airfoils create the lift force by means of fluid movement. The flying of aircrafts, generation of electricity through turbines, extraction of water from wells and many other applications are achieved by the lift force of the airfoil. The amount of lift force depends on the geometry of the airfoil. Since any change in the geometry of an airfoil directly affects the flow dynamics over it, The desired change can be made using the following terms through which the airfoil profiles are modeled. In Figure 1, a and U_∞

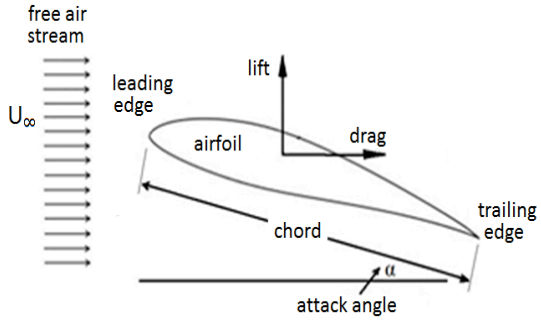

Fig. 1 Airfoil profile and related terms refer to attack angle and free stream velocity, respectively.

What is expected of an airfoil is that it provides high lift force and low drag force. Fig. 1 shows that the net force in the y direction generates the lift force and the net force in the x direction generates the drag force. These net forces are determined by integrating the wall shear stress and wall pressure forces over the wall surface of the airfoil. What differs an airfoil from others is the performance it shows in different flow conditions. The performance of an airfoil is defined as the ratio of lift force to drag force. The flow dynamics of airfoils is commonly defined by dimensionless coefficients. The lift coefficient, drag coefficient and pressure coefficient are the dimensionless coefficients of lift force, drag force and pressure, respectively.

Lift coefficient $$: C_L = \frac{F_L}{0.5\rho U_\infty^2 A}$$

Drag coefficient $$: C_D = \frac{F_D}{0.5\rho U_\infty^2 A}$$

Pressure coefficient $$: C_P = \frac{P - P_\infty}{0.5\rho U_\infty^2}$$

Here, P is the absolute fluid pressure acting on the airfoil wall, P_∞ is the local atmospheric pressure, U_∞ is the free stream velocity, A is the airfoil shade area specified as the multiplication of chord length and airfoil width, and F_L and F_D are the lift and drag forces, respectively. Since the performance of an airfoil is the ratio of lift force to drag force, it can also be determined as the ratio of lift coefficient to drag coefficient (C_L / C_D).

2. Numerical Solution Method

The two-dimensional cartesian coordinates of airfoil profiles were provided online and the downloaded profiles are referred to as FX 84-W-218, Selig S8036, FX-63-137,

EPPLER 58 and GOE 795. These profiles were the models of a chord length of one meter.

First, a solid airfoil geometry was generated using the two-dimensional Cartesian coordinates of these profiles. Then an air domain surrounding the airfoil was constructed. The outer boundary of the flow domain was kept very far away from the airfoil where the viscous effects can be negligible. Since CFX is not capable of solving the two-dimensional flows, the flow field was extended to a third direction with a cell thickness of one mesh so that the two-dimensional flow could be performed. A thin air flow domain was obtained by subtracting the solid airfoil geometry. The airfoil walls contacting the flow domain were set as wall boundary conditions, and the right and left faces of the thin flow domain were set as symmetry boundary conditions. The inlet and outlet boundaries of the flow domain, as illustrated in Figure 2, were set as velocity inlet and pressure outlet boundary conditions, respectively. Along the inlet boundary, the flow is at free stream velocity, and along the outlet boundary, the flow is opened to atmosphere where the gauge pressure is zero.

The flow domain is divided into numerous small flow cells for the numerical solution. The mesh in the flow field is compacted near the walls for boundary layer resolution and compacted in the trail region behind the airfoil tail to solve the flow properties well due to rapid spatial change in these regions and mesh resolution are rarefied at the other regions due to the flow properties. Doing this, the mesh element numbers are kept at minimum. Low-Reynolds-number turbulent models are selected for the turbulent flow solution. Therefore, the near wall mesh resolution is increased according to the dimensionless distance specified as $y^+<1$. Fig. 3 shows the constructed mesh, indicating high mesh density around the airfoil and in the tail trail region.

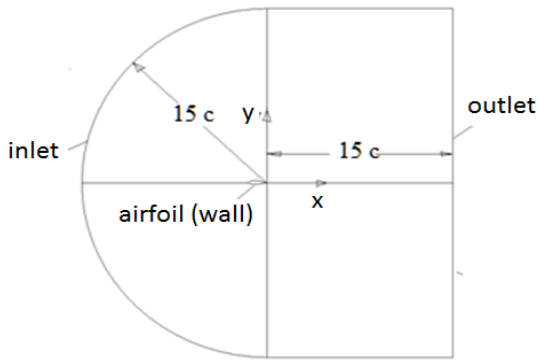

Fig. 2 Flow field boundaries over airfoil

According to the unstructured mesh, all flow domains include a mesh element number ranging from 5.10^5 to 7.10^5. Showing the value between last two iterations, the absolute value of convergence criteria is selected as $\varepsilon = 10^{-7}$ in order to provide a convergent solution.

A laminar flow region can be categorized as steady or unsteady depending on the mass flow rate changes with time, however, a turbulent flow field is always unsteady whether the mass flow rate changes or not

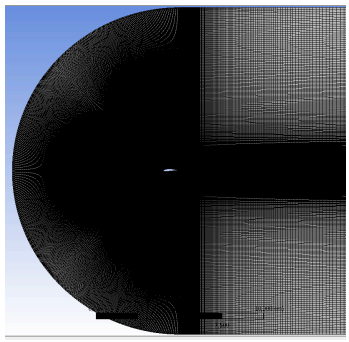

Fig. 3 Mesh of the computational domain

. This is due to the fact that it includes many vortex motions ranging from small to large ones. These vortex motions grow and dissipate temporarily and spatially in the flow field. The solution of an unsteady turbulent flow is only possible with direct numerical simulation (DNS), which, however, requires high mesh resolutions and small-time steps to be able to simulate the smallest vortex motion growing in flow fields temporarily and spatially. It is therefore impossible to simulate directly the flows except for the simple flows with today's computers. To simply solve the turbulent flow, the unsteady turbulent flow can be assessed over the time- average effects. Doing this, the turbulent flow is reduced to a steady flow. Thus, the basic flow equations of which the time average (mean) is calculated are converted to Reynolds averaged Navier-Stokes (RANS) equations. Equ.1 shows the mean momentum equation in the x direction for sample representations.

$$\rho\left(\frac{\partial \bar{u}}{\partial t}+\bar{u}\frac{\partial \bar{u}}{\partial x}+\bar{v}\frac{\partial \bar{u}}{\partial y}+\bar{w}\frac{\partial \bar{u}}{\partial z}\right)=-\frac{\partial \bar{P}}{\partial x}+\rho g_x + \mu\nabla^2\bar{u}-\rho\left(\frac{\partial \overline{u'^2}}{\partial x}+\frac{\partial \overline{u'v'}}{\partial y}+\frac{\partial \overline{u'w'}}{\partial z}\right) \quad (1)$$

According to the basic flow equations, additional turbulent shear stresses ($-\rho\overline{u'v'}$, $-\rho\overline{u'^2}$, $-\rho\overline{u'w'}$) are present in the RANS equations. These stresses are referred to as Reynolds stresses or turbulent stresses. Reynolds stresses are the only unknowns in the RANS equations. Many turbulent models have been proposed to numerically simulate the flow and to solve these Reynolds stresses. In this study, SST k-omega model is the model of choice for turbulent flows over airfoils. Here, the air flow on turbine airfoils can be categorized as a steady, compressible and isothermal flow with a Newtonian fluid. In addition to continuity and RANS equations, the energy equation is also activated to take into account the compressible flow effects and viscous effects on pressure and temperature of the air ideal gas.

2.1. Validation of Numerical Solution

Before a numerical analysis is performed, numerical results must be validated with the experimental data to make sure that the flow simulation is predictive. The experimental data of NACA0012 and NACA2412 profiles were utilized for comparison. In parallel to the experimental study, numerical solutions were performed

© IJRED – ISSN: 2252-4940, July 15th 2018, All rights reserved

for the two profiles. Table 1 and Fig. 4 present the comparison of numerical results with experimental data for NACA2412 and NACA0012, respectively. Table 1 shows good agreement between the numerical values and the experimental data, which ensures the credibility of the numerical solutions. The comparison of numerical values with experimental data of NACA 0012 is plotted in Fig. 4 in terms of flow pressure variation along the upper and lower walls. The good fit in Fig. 4 between the pressure curves and the experimental data at both walls also ensures the credibility of the numerical solutions.

Table 1
Comparison of experimental and numerical C_L values for NACA2412

Attack Angle (α)	Experimental	Numerical
-4°	-0.20	-0.1930
4°	0.650	0.6520
12°	1.40	1.4370
15°	1.60	1.650
20°	1.20	---

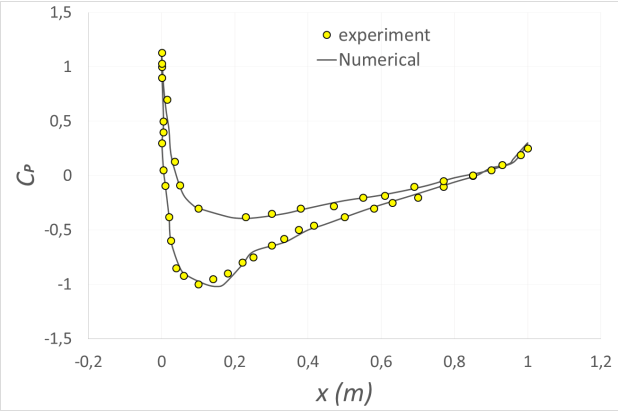

Fig. 4 Comparison of experimental and numerical pressure coefficients for NACA0012

3. Airfoil Performance Assessment

Following the validation of the numerical simulations in Table 1 and Fig. 4, the numerical simulations performed for each airfoil can be analyzed using dimensionless parameters. Performance curves varying under different attack angle and wind speed conditions have been illustrated for each airfoil in Fig. 5, indicating a peak value in the performance curves at attack angles between 4° and 7°. An inference can be drawn that the wind turbines were most efficient at these attack angles where the performance was highest. As shown in Fig. 5, the performance of all airfoil becomes optimum at attack angles between 4° and 7°. EPPLER 58 and FX 63-137 profiles showed better performance than the other profiles at attack angles between 0° and 7°. The performance variations with wind speed indicate that the performance curves rise to a high level at about a constant rate as the wind speed increases. However, this constant rate is different at every attack angle and for each profile. For example, the constant rate in EPPLER 58 is high at low attack angles whereas the constant rate in Selig S8036 is high at medium attack angles. To sum up, it can be stated that wind turbines become more efficient when the wind speed increases.

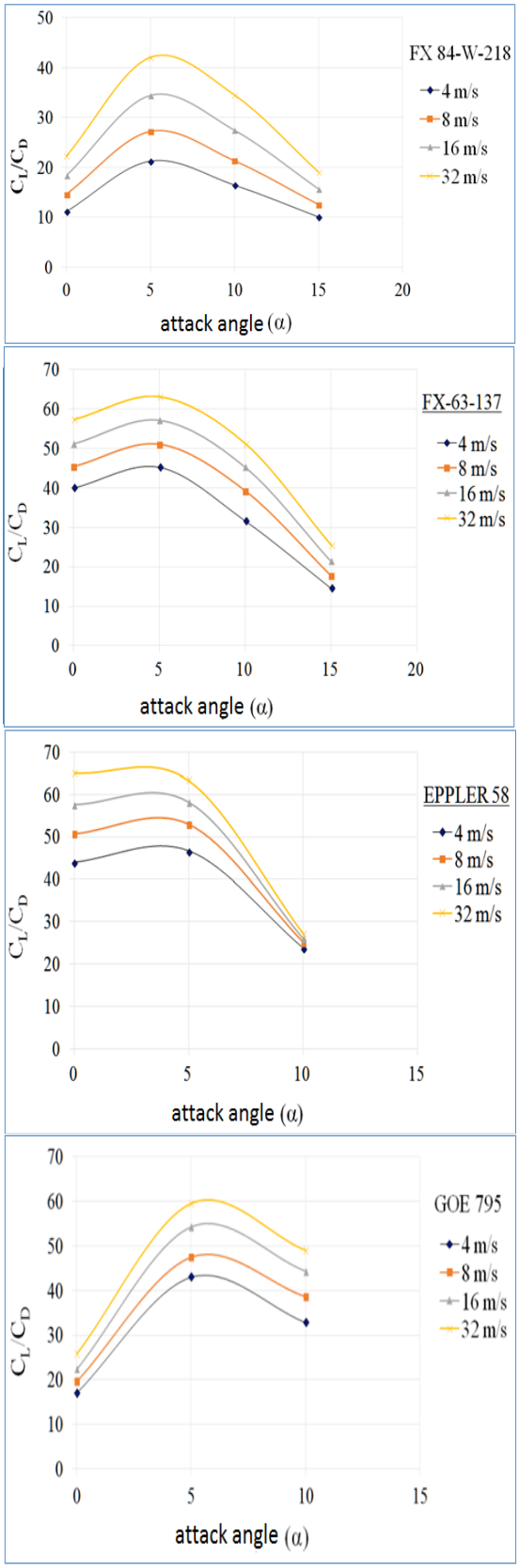

Fig. 5 Performance variation under different attack angle and wind speed conditions at each airfoil

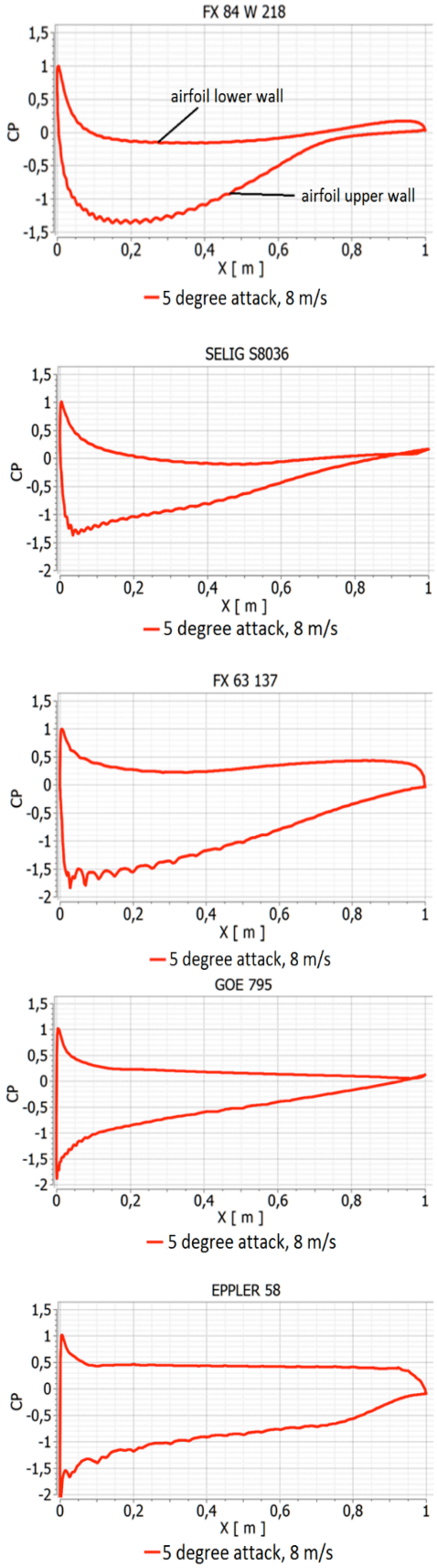

Fig. 6 Distribution of pressure on upper and bottom walls at attack angle of 5° and wind speed of 8 m/s for each five airfoils

The pressure distribution on the upper and bottom walls of airfoils in flows has been illustrated in Fig. 6. The pressure distribution has been plotted only for the attack angle of 5° and wind speed of 8 m/s. The lift force on the airfoil is a result of the pressure difference between the upper and bottom walls and including the wall shear effect. According to the Bernoulli equation, pressure decreases with an increase in flow speed while pressure increases with a decrease in flow speed in outer flow field. Pressure distribution on airfoils are commonly defined by pressure coefficients.

The positive and negative values of the pressure coefficient curves on the upper and bottom walls in Fig. 6 indicate that the pressure on the upper wall is under atmospheric pressure and that the pressure on the bottom wall is over atmospheric pressure along the chord length. Negative coefficients denote the vacuum pressure while positive coefficients denote the gauge pressure. The closed area between the upper and bottom curves shows the difference in pressure. The size of that area represents the lift force size.

It can be observed from Fig. 6 that the vacuum pressure distribution is higher on the upper wall of FX-63-137 and the gauge pressure distribution is higher on the bottom wall of EPPLER 58 profiles when compared to those of other profiles. These advantages can be exploited by generating a new profile from the upper and lower profile curves of both airfoils. The upper wall coordinates of FX-63-137 and the bottom wall coordinates of EPPLER 58 can be integrated to generate the new profile, which is referred to as hybrid profile and shown in Figure 7.

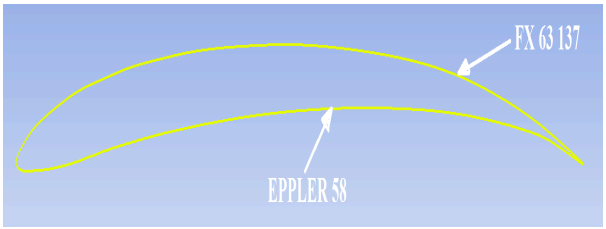

Fig. 7. Hybrid profile consisting of FX-63-137 and EPPLER 58

To assess the effect of air flow on hybrid performance, flows at attack angles and wind speeds were simulated using numerical solutions. The variation in performance with different attack angles and wind speeds was illustrated in Fig. 8 for all simulated airfoils after the numerical results were obtained for the hybrid airfoil. The variation in performance with different attack angles was illustrated in Fig. 8 in order to obtain the best profiles which yield the best performance. In addition, performance curves with attack angles were plotted for each wind speed. Thick and dashed line in Fig. 8 represents the hybrid performance curve.

Figures show that all airfoils reach a peak in performance at attack angles between 4° and 7°. The comparison of the performance curves of EPPLER 58, Hybrid and FX-63-137 at low attack angles less than 5° indicates that EPPLER 58 curve is very close to the hybrid curve and higher than FX-63-137 curve with an amount of 11% at zero attack angle but that the amount starts to decrease and eventually becomes equal towards the attack angle of 5°. The performance of EPPLER 58 is better than that of other profiles at attack angles less than 5°, however, it declines rapidly at attack angles above 5°. The performance of the hybrid and FX-63-137 also declines but not as much as that of EPPLER 58. The performance curves of GOE 795 and FX-63-137 are similar to each other at attack angles

© IJRED – ISSN: 2252-4940, July 15th 2018, All rights reserved

between 6° and 10°, however, a little lower than that of the hybrid with a maximum value of %5.6. All in all, their performance is better than that of the other profiles within the given range of attack angles. SELIG S8036 performs well at attack angles above 7° followed by a steady-state with nearly-constant values. Fig. 8 also shows that FX 84-W-218 with the lowest performance curves at all attack angles yields the worst performance of all profiles. For all simulations in Fig. 8, values 15 and 65 denote the minimum and maximum performance, respectively.

As expected, the hybrid profile achieved better performance than EPPLER 58 and FX-63-137 at some certain angle attacks. The analysis of the performance curves at each wind speed indicates that the performance curve of the hybrid follows that of EPPLER 58 and that the maximum difference between the two is 3% at attack angles less than 6° and at wind speeds of 4, 8 and 16 m/s. On the other hand, the performance curve of the hybrid is very close to that of FX-63-137 at wind speeds of 4, 8 and 16 m/s.

At the highest wind speed (32 m/s), the performance curve of the hybrid has slightly lower values than that of EPPLER 58 and FX-63-137 at attack angles less than5° and above 10°, respectively. Table 2 presents the deviations (%) in the performance of the hybrid, EPPLER 58 and FX-63-137 at all attack angles, indicating that the hybrid profile has better performance than FX-63-137 (maximum difference being 5.6%) and EPPLER 58 (maximum difference being 3.5%) at the attack angle of 5°. Table 2 also shows that the hybrid profile has better performance than EPPLER 58 and FX-63-137 at attack angles between 5° and 10°. The hybrid profile has better performance than EPPLER 58 and FX-63-137 at attack angles between 5° and 10°. Eliminating the disadvantages of EPPLER 58 and FX-63-137, the hybrid profile also has a more stable performance at other attack angles.

Table 2
Deviations (%) in hybrid airfoil performance

Deviations (%) between Hybrid and EPPLER 58				
α/(m/s)	**0°**	**5°**	**10°**	**15°**
4	-0.05	2.31	41.26	---------
8	-2.33	0.99	60.06	---------
16	-2.86	2.40	76.76	---------
32	-3.97	3.51	86.76	---------
Deviations (%) between Hybrid and FX 63 137				
4	10.03	5.60	6.16	-3.92
8	9.28	4.95	2.62	-8.24
16	9.36	4.27	1.67	-12.43
32	9.03	3.86	-0.99	-17.77

Fig.9 illustrates the pressure distribution on hybrid, EPPLER 58 and FX-63-137 walls for comparison. The pressure distribution of the hybrid profile (the upper wall coordinates of FX-63-137 and the bottom wall coordinates of EPPLER 58) shows that the upper wall pressure distribution is the same as that of FX-63-137 and that the lower wall pressure distribution is the same as that of EPPLER 58. An inference can be drawn that flow dynamics on upper and lower walls do not affect each other. Any profile, the lower wall of which is modified, will have the same flow behavior on the upper wall.

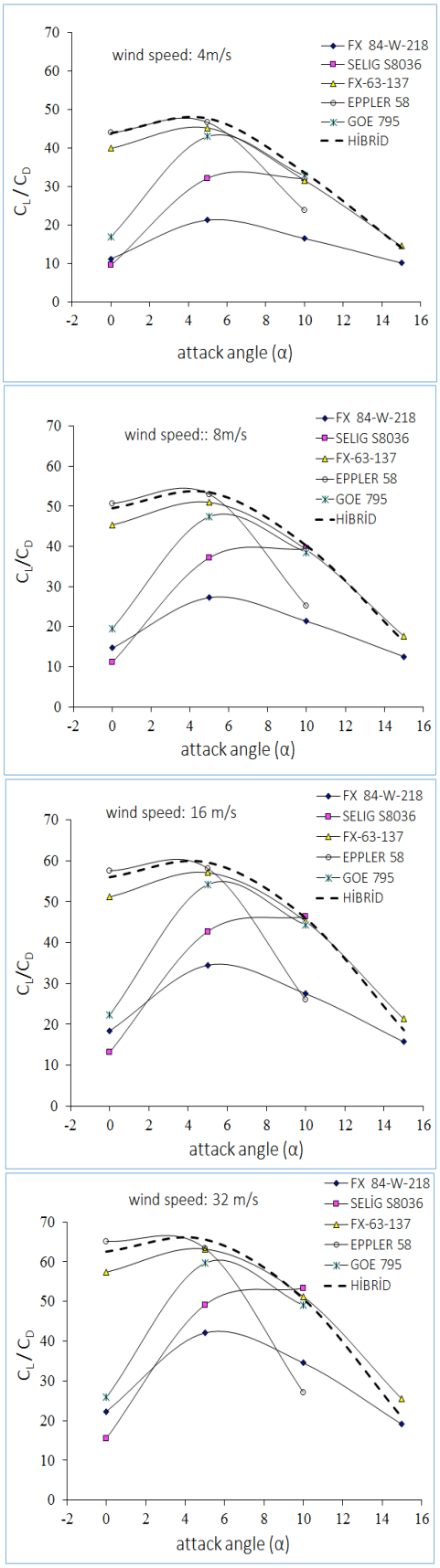

Fig. 8 Comparison of performance of hybrid airfoil with that of other airfoils at different wind speeds

As can be seen, it is possible to generate high-performance airfoils by analyzing the pressure distribution

on upper and lower walls of airfoils, each of which achieves the best performance. Consequently, the hybrid profile eliminates the disadvantages of EPPLER 58 and FX-63-137 for any given wind speeds and is more stable than them at attack angles where they yield bad performance

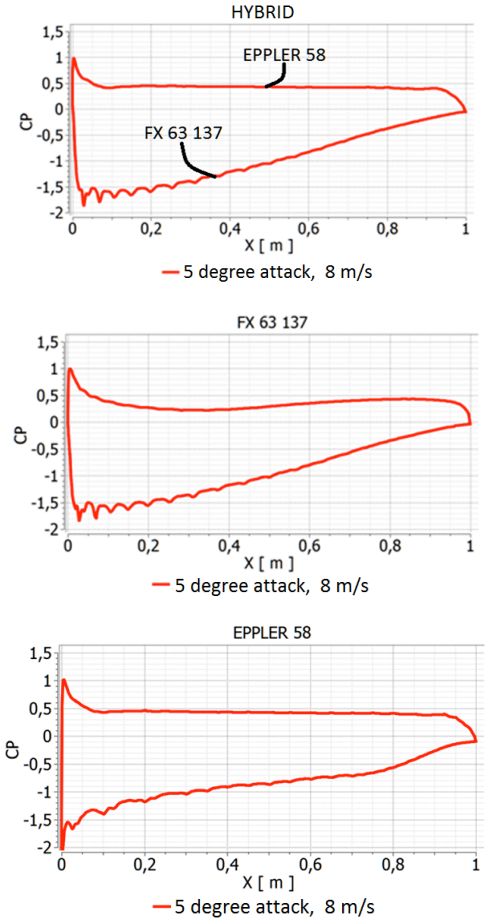

Fig. 9 Comparison of pressure coefficient of hybrid profile with those of EPPLER 58 and FX-63-137

4. Conclusion

This study numerically investigated differ-rent types of airfoils in terms of performance to increase the efficiency of wind turbines. The turbulent flow over airfoils was solved using the mean basic flow equations (RANS). The Reynolds stresses in RANS equations were solved using shear stress transport (SST) k-omega model. The flows over the selected airfoil were numerically performed at different attack angles ($0^o < \alpha < 20^o$) and different wind speeds (4, 8, 16 and 32 m/s). Numerical results show an improvement in airfoil performance directly proportional to wind speed. They also show that all airfoils reach a peak in performance at attack angles between 4^o and 7^o. EPPLER 58 airfoil profile has slightly higher performance (60 C_L / C_D) than FX 63-137 but much higher performance than other profiles at low attack angles ($\alpha < 6^o$). While FX 63-137 and GOE 795 have better performance (between 50 and 60 C_L / C_D) than others at attack angles between 7^o and 10^o, Selig S8036 has high performance (between 50 and 55 C_L / C_D) at high attack angles.

The pressure distribution on the upper wall of EPPLER 58 and lower wall of FX-63-137 was the best. Therefore, a hybrid profile was generated using their wall coordinates. The hybrid profile has better performance (maximum difference being 6%) than EPPLER 58 and FX-63-137 at attack angles between 5^o and 10^o, and is closer to the highest performance curves at other attack angles. As a consequence, this study shows that high-performance airfoil profiles can be generated by numerically analyzing pressure distribution on airfoil surfaces.

References

Bekka, N., Bessaih, R., Sellam, M., Chpoun, A. (2009). Numerical study of heat transfer around the small scale airfoil using various turbulence models. Numerical Heat Transfer, Part A: Applications. 56(12), 946-969

Bertagnolio, F., Sorensen, N.N., &Rasmussen. (2005). F. New insight into the flow around a wind turbine airfoil section. J. Solar Energy-Trans. ASME. 217(2): 214-222

Bermudez, L., Velazquez, A., Matesans, A. (2002). Viscous–inviscid method for the simulation of turbulent unsteady wind turbine airfoil flow. Journal of Wind Engineering&Industrial Aerodynamics. 90, 6, 643-661.

Dahlstrom, S., &Davidson, L. (2000). Large Eddy Simulation of the flow around an aerospatiale A-aerofoil. ECCOMAS 2000, European Congress on Computational Methods in Applied Sciences and Engi-neering. Barcelona, Spain, 11-14 Septem-ber 2000.

Geissler, W. (2003). Numerical study of buffet and transonic flutter on the NLR 7301 airfoil. Aerospace Science and Technology. 7:40-550.

Güleren, K.M., Demir, S. (2011). Rüzgâr türbinleri için düşük hücum açılarında farklı kanat profillerinin performans analizi. Journal of Thermal Science and Technoloji *31, 2, 51-59*

Jang, C.S., Ross, J.C., &Cummings, R.M. (1998). Numerical investigation of an airfoil with a gurney flap. Aircraft Design. 1(2), 75-85.

Ji, Y., Weibin, Y., &jianliang. W. (2012). Numerical simulation of aerodynamic performance for two-dimensional wind turbine airfoils. International Conference on Advances in Computatio-nal Modeling and Simulation. Procedia Engineering. 31, 80 – 86

King, L.S., Johnson, D.A. (1985). Separated transonic airfoil flow calculations with a non-equilibrium turbulence model. NASA Technical Resports, NASA Ames Research Center; Moffett Field, CA, United States, NASA TM 86830.

Parezanovic, V., Rasuo, B., &Adzic, M. (2006) Design of airfoils for wind turbine blades. The French-Serbian European Summer University: Renewable Energy Sources and Environment-Multidisciplinary Aspect. 17-24 October 2006, Rnjačka Banja, Serbia.

Selig, M.S., &Granahan B.D.M. (2003). Wind tunnel aerodynamic tests of six airfoils for use on small wind turbines. *National Renewable Energy Laboratory (NREL)*, 1617 Cole Boulevard, Golden, Colorado 80401-3393 303-275-3000. *www.nrel.gov*. Period of Performance: October 31, 2002–January 31 2003.

UIUC Applied Aerodynamics Group. UIUC Airfoil Coordinates Database (2017). http://m-selig.ae.illinois.edu/ads/coord_database.html, Accessed March 3, 2017

Tangler, J.T., Somers, D.M. (1995). NREL Airfoil Families for HAWTs. Proc. WINDPOWER'95. Washington DC ABD;117-123.

Yılmaz, İ., Çam, Ö., Taştan, M., Karcı, A. (2016) Farklı rüzgar türbin kanat profillerinin aerodinamik performansinin deneysel incelenmesi. Politeknik Dergisi. Cilt 19, Sayı 4, 577-584

© IJRED – ISSN: 2252-4940, July 15th 2018, All rights reserved